HYDROLOGICAL PROCESSES
Hydrol. Process. **21**, 705–716 (2007)
Published online 14 September 2006 in Wiley InterScience
(www.interscience.wiley.com) DOI: 10.1002/hyp.6407

On the winter evolution of snow thermophysical properties over land-fast first-year sea ice

Alexandre Langlois,* C. J. Mundy and David G. Barber
Centre for Earth Observation Science (CEOS), Faculty of Environment, University of Manitoba, Winnipeg, MB, Canada

Abstract:

The geophysical, thermodynamic and dielectric properties of snow are important state variables that are known to be sensitive to Arctic climate variability and change. Given recent observations of changes in the Arctic physical system (Arctic Climate Impact Assessment, 2004), it is important to focus on the processes that give rise to variability in the horizontal, vertical and temporal dimensions of the life-history of snow on sea ice. The objectives in this study are to present these 'state' variables and to investigate the processes that govern variability in the vertical, horizontal and temporal dimension by using a case study over land-fast first-year sea ice for the period December 2003 to June 2004.

Results from two sampling areas (thin and thick snowpacks) show that differences in snowpack thickness can substantially change the vertical and temporal evolution of snow properties. During the late fall and early winter (cooling period) we measured no significant changes in the physical properties, except for thin snow-cover salinity, which decreased throughout the period. Fall-snow desalination was only observed under thin snowpacks with a rate of $-0{\cdot}12$ ppt day^{-1}. Significant changes occurred in the late winter and early spring (warming period), especially for snow grain size. Snow grain kinetic growth of $0{\cdot}25$–$0{\cdot}48$ mm·day^{-1} was measured coincidently with increasing salinity and wetness for both thin and thick snowpacks.

KEY WORDS snow cover; physical properties; electrical properties; vertical evolution; first-year sea ice; CASES

Received 8 June 2005; Accepted 7 March 2006

INTRODUCTION

Snow plays a central role inhibiting the transfer of energy, gas and mass across the ocean–sea-ice–atmosphere (OSA) interface (Arons and Colbeck, 1995). An adequate method for the direct measurement or modelling of either snow state variables (thickness, distribution) or the physical evolution of snow on sea ice (metamorphism, brine migration, etc.) has yet to be developed. One of the primary difficulties is the various spatial and temporal scales over which snow varies in the Arctic (Barber *et al*., 1995). Of particular relevance is the nearly complete absence of winter-season snow measurements from a fixed location complete with ancillary measurements of surface energy balance, meteorological observations and thermodynamic processes operating through the snow–sea-ice system. To constrain this introduction, we briefly provide an assessment of the state of snow science on sea ice, focusing on energy transfer within the snow–sea-ice system, in particular on (a) conductive fluxes, (b) radiative transfer, and (c) snow grain metamorphism and bulk geophysics.

Studies of conductive transfer in snow-covered sea ice (e.g. Eicken *et al*., 1995; Sturm *et al*., 2002) have shown that snow controls thermal conduction k_s through the snow–sea-ice system. The thermal conductivity of snow is usually computed from statistical models relating k_s to snow density ρ_s and is inversely proportional to vapour flow, a fundamental parameter in energy exchange and metamorphic processes within the snow cover (e.g. Colbeck, 1993; Sturm *et al*., 2002). *In situ* measurements of k_s by Sturm *et al*. (2002) ranged between $0{\cdot}078$ and $0{\cdot}290$ W m^{-1} K^{-1}, with a bulk average of $0{\cdot}14$ W m^{-1} K^{-1}, showing that air movements within the snow cover also play an important role in heat and mass transfer (Granberg, 1998).

It is also well known that snow structure and density affect thermal conductivity (e.g. Mellor, 1977; Sturm *et al*., 1997). Seasonal snow density values have been widely published (e.g. Vowinkel and Orvig, 1970; Barber *et al*., 1994; Warren *et al*., 1999), but detailed snow grain metamorphism observations are very limited, as scientists struggled for many years to characterize the geometry of snow (Arons and Colbeck, 1995). Previous research has shown that kinetic growth grains dominate the basal layers and more rounded grains typically occur within the upper layers of snow on sea ice (Barber *et al*., 1995). Wu *et al*. (1999) noted the lack of information on snow geometry variation and evolution, arguing that improved observations are needed to parameterize the snow thermal conductivity correctly (Massom *et al*., 2001; Sturm *et al*., 2002; Eicken, 2003).

Energy fluxes have a dominant influence on snowpack evolution, including metamorphism and water phase transitions (Barber *et al*., 1994). Net shortwave radiation ($K^* = K\downarrow - K\uparrow$) is highly influenced by the presence or

* Correspondence to: Alexandre Langlois, Centre for Earth Observation Science (CEOS), Department of Environment and Geography, Faculty of Environment, University of Manitoba, Winnipeg, MB R3T 2N2, Canada.
E-mail: umlangl2@cc.umanitoba.ca

absence of snow over sea ice. The high albedo of snow significantly reduces absorbed downwelling shortwave radiation $K\downarrow$ and fresh snowfall can significantly increase the surface albedo, particularly in the near-infrared portions of the spectrum (Li *et al.*, 2001). Radiative transfer of shortwave energy is dominated by grain size and shape (e.g. Warren, 1982; Zhou and Li, 2002). The presence of small amounts of liquid-phase water can also have a dramatic effect on increasing shortwave transmission within naturally occurring snow on sea ice (Yang *et al.*, 1999).

The net longwave flux ($L^* = L\downarrow - L\uparrow$) is determined by the temperature and humidity profile in the lower atmosphere and the surface temperature of the snow (Hanesiak *et al.*, 1999). The open ocean, melt ponds and melting snow of spring and summer will increase cloud fraction, increasing the amount of downwelling longwave radiation during the summer (Barber and Thomas, 1998). Sensitivities of melt onset to cloud fraction (CF), base height and phase transitions in the snow are the topic of contemporary research outside of the scope of this paper (e.g. Curry *et al.* 1996; Xin and Barber, 2006).

Snow on land has been studied extensively, whereas equivalent studies of snow on sea ice are very much in their infancy (e.g. Barber *et al.*, 1995; Sturm *et al.*, 2002). Of the snow-on-sea-ice work, almost all of the previous studies have focused on the spring to summer transition rather than on the important fall to winter or the winter to spring transitions. An accelerated hydrological cycle, as modelled under an increased CO_2 and aerosol scenario (Boer *et al.*, 2000), would increase the amount of snowfall, given the expected climatology of sea-ice-covered oceans (Flato and Boer, 2001). Therefore, snow on sea ice remains a high priority for field, modelling and process-related studies pertaining to sea ice and climate change (Houghton *et al.*, 2001). Of high priority is an examination of the observed climate states of the snow–sea-ice system. These climate states are those that affect the transfer of mass, gas, and energy across the OSA and, thus, control how the OSA will respond to projected climate variability and change at high latitudes. Recent studies reveal that the sea ice extent continues to decrease for the Arctic basin (Stroeve *et al.*, 2005). Also, the patterns in sea-ice concentration and areal extent show a statistically significant trend toward negative anomalies throughout the period 1979 to 2000 (Barber and Hanesiak, 2004). Projections suggest that the Arctic Ocean will be covered by seasonal ice as early as 2050 (Flato and Boer, 2001).

In this paper we examine the state of the snow system as a temporal case study over the winter period. These measurements are coupled with *in situ* estimates of conductive and radiative fluxes as a means to illuminate the role of these forcing variables on thermophysical properties of the evolving snow cover. We have selected land-fast first-year sea ice because it is a stable platform upon which we can conduct replicate sampling and because first-year sea-ice types are becoming increasingly important as we lose multiyear forms of sea ice (Comiso, 2002). To constrain our analysis we focus on two objectives: (a) characterizing the vertical and seasonal profiles of snow physical properties over first-year sea ice; (b) investigating the thermodynamic and radiative processes that affect these properties. We present both the physical and thermodynamic processes of the snow on sea ice with a level of detail so far missing in the literature and which is necessary for development of numerical snow models.

METHODS

Study site

Snow data were collected during the Canadian Arctic Shelf Exchange Study (CASES) overwintering mission (26 November 2003 (day 329) continuously until 12 May 2004 (day 132)). During the study period, the Canadian Coast Guard research icebreaker *CCGS Amundsen* (a class 1200 icebreaker) was frozen into land-fast smooth first-year sea ice about 20 km offshore in Franklin Bay, Northwest Territories, Canada (Figure 1). The sea ice surrounding the ship was 80 cm thick on 5 December 2003 and had grown to 210 cm by 31 May 2004.

Maykut and Church (1973) reported that the minimum monthly air temperature for this region was $-28\,^{\circ}\mathrm{C}$ for February and the maximum $3{\cdot}9\,^{\circ}\mathrm{C}$ for July, arranged between 1931 and 1966. Monthly mean vertically integrated precipitable water ranges from 2·9 mm in February and March to 16·2 mm in July (Serreze *et al.*, 1995; Curry *et al.*, 1996).

Meteorological observations

Daily average air temperature and wind speed were calculated from hourly observations from the AXYS Automated Voluntary Observation Ship (AVOS) system on the roof of the ship's wheelhouse, minimizing the ship's influence (approximately 20 m above the sea ice). The AVOS is an interactive environmental reporting system that allows ships to transmit current meteorological observations to a central land station every hour. Measurements are updated every 10 min and displayed on a computer monitor located in the wheelhouse (Fisico, 2005). Cloud amount was monitored by an observer on a scale from 1 to 8 (0 is a clear sky and 8 is overcast).

Layer gradients and energy fluxes

Saturation vapour pressure e_{si} and temperature vertical differences were calculated from temperatures measured within the snowpack. The three main constituents of snow over sea ice are ice, liquid water (brine) and air. The average volume percentages of these constituents over the study period are 18–20%, 1–2% and 78–80% for ice, brine and air respectively. Therefore, for this study, we considered the saturation vapour pressure of ice e_{si} as

$$e_{si} = A\mathrm{e}^{-B/T} \tag{1}$$

where A and B are pressure and temperature constants according to ice and T (K) is the volume temperature

DOI: 10.1002/hyp

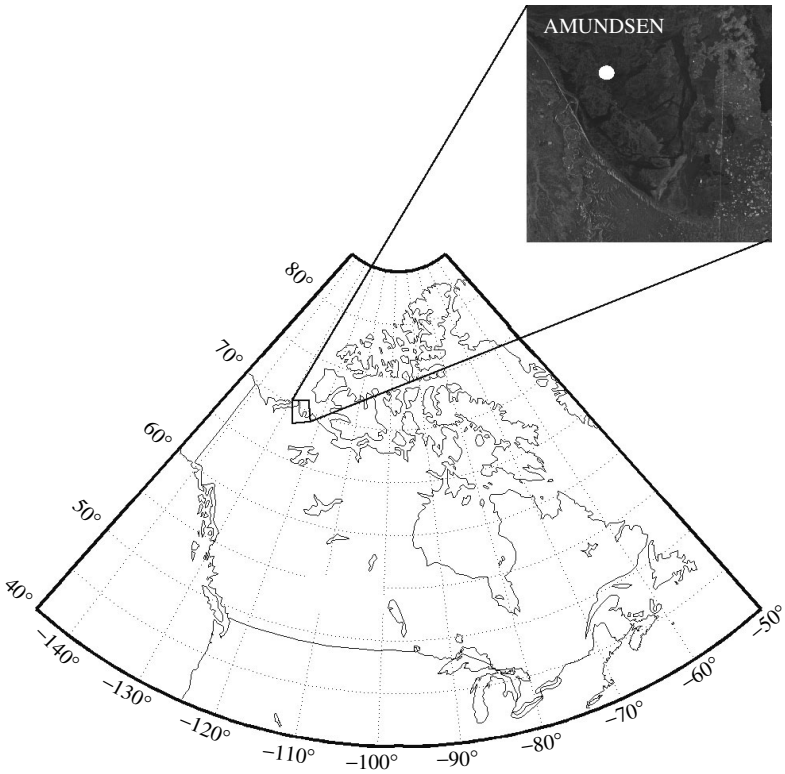

Figure 1. Overwintering study area with inset of RADARSAT scanSAR data showing the location where the *CCGS Amundsen* was frozen in Franklin Bay, NWT

(Rogers and Yau, 1989). Since we rescaled the snow depth from centimetres to layers within the thin and thick snow sampling area (see 'Vertical profile characterization' section), we calculate the vertical difference between layers L for volume temperatures $\delta T/\delta_L$ and saturation vapour pressure $\delta e_{\mathrm{si}}/\delta_L$, hereafter referred to as 'layer gradients'.

Net all-wave radiation Q^* and its longwave L^* and shortwave K^* components were measured at a meteorological station located 1·6 km east of the ship (70°2·516′N, 126°15·894′W). Net shortwave K^* and longwave L^* radiation were determined from the difference between observed downwelling and upwelling radiation using Eppley pyranometers and pyrageometers respectively. Sensor output was scanned at three standard deviation intervals and stored as 10 min averages by a Campbell Scientific (model 21X) data logger. Data collection occurred between 23 January (day 23) and 7 May 2004 (day 127).

Snow properties

Physical properties. Snow physical properties were collected at a sampling site located adjacent to the ship on the north side (ship orientation 106°). This site consisted of a 50 m × 50 m zone of undisturbed snow. Snow pits were excavated diurnally (morning, noon and afternoon) every second day at areas of thin (4–10 cm) and thick (10–80 cm) snow covers between 6 December 2003 and 7 May 2004. We arranged the sampling so that thin and thick snowpacks would be sampled throughout the study period.

Temperature profiles were first measured in the excavated snow pits using a Hart Scientific temperature probe with a published accuracy of ±0·025 °C over a temperature range of −200 to +100 °C. We used a dielectric method to compute snow wetness (Wv (%)). This technique uses a capacitance plate, which measures the increased conductivity due to small amounts of water in the liquid phase. This technique has an estimated sensitivity of 0·5% water by volume when there is no brine in the snow layer. The technique is unable to measure Wv in the highly brine-saturated basal layer of snow on first-year sea ice forms due to the elevated dielectric constant of this volume and the lack of suitable calibration. Further details are available in Barber *et al.* (1995). Snow samples were extracted at 2 cm intervals from the surface to the snow–ice interface with a 66·36 cm^3 density cutter. Each sample was weighed using a Denver Instrument digital scale accurate to obtain density, and melted for salinity measurements using a WTW conductivity meter. Prior to melting, subsamples were photographed in a cold room (−15 to −25 °C) to measure snow grain size and structure. Subsamples were first placed on a 2 mm gridded plate and photographed to measure the average snow grain size of the sample. Individual grains were then randomly extracted from the grid plate and placed in chemically inactive and optically transparent silicone oil for microstructural photographs. All pictures were taken with a Canon PowerShot 4·2 megapixel camera mounted on a Leica MZ 7·5 stereomicroscope. Snow grain photographs were analysed in MatLab using a specially designed polygon analysis code, which extracted

DOI: 10.1002/hyp

snow grain size and structure (e.g. major and minor axes and area). Brine volume was also computed from salinity and temperature for each layer of the snowpack, following a method by Frankenstein and Garner (1967). The fractional volume of brine within the snow was calculated according to Cox and Weeks (1982).

Vertical profile characterization. Thin snow was treated as one group, since the thickness was stable over the study period. With 2 cm thickness snow samples, thin snow pits were limited to three layers (top, middle and bottom) throughout the study period, as most of the snow pits were 6 cm thick. The thick snowpacks were separated into three different groups as the thickness evolved throughout the study period. The behaviour of physical properties is quite different for a 20 cm to an 80 cm snowpack as was observed in the thick snow cover classes. A 'Tukey' *post hoc* analysis of variance (Moore and McCabe, 1993) was conducted to test whether these layers were statistically different from one another for both thin and thick snowpacks. The results showed that all layers were statistically different for at least two physical properties at the 95% confidence interval. Therefore, snow pits at the thick site were standardized to a scale from 0 to 1 to permit comparison of the same layers throughout the season.

RESULTS AND DISCUSSION

Snow depth at the thin snow site varied only a small amount over the course of the study period. The thick snow site, however, showed a stepwise increase due to depositional events (Figure 2a). Three major snow events, due to snowfall and/or redistribution, occurred during the overwintering period (days 5, 42 and 91), and are circled in Figure 2b. These snow events lead to the delineation of three different thickness groups (10–25, 25–45 and 45–80 cm) used in the analysis for thick snowpacks. The first group included four layers (L1 to L4) until the first snow accumulation that added two layers (L5 and L6) on day 42. Finally, one last depositional event added two more layers (L7 and L8) on day 91 (Figure 2b). Air temperature from the meteorological station aboard the ship was our marker for the temporal analysis. We separated the overwinter mission into two thermal regimes: the cooling period and the warming period separated on day 59, when the minimum air temperature was recorded at the AVOS station (Figure 3a).

Cooling period

Meteorological observations, vapour pressure and energy fluxes. The air temperature was variable during the cooling period from day 343 to day 59, with a maximum of $-11{\cdot}2\,^{\circ}\mathrm{C}$ measured on day 5. A marked decrease was observed between days 5 and 9, where the temperature dropped to $-32{\cdot}6\,^{\circ}\mathrm{C}$ and stayed relatively cold until the minimum on day 59. Winds had a significant impact on snow redistribution throughout the period (Figure 2b). The second snow redistribution event occurred on day 42, when winds reached a daily average of 10 m s^{-1} between days 38 and 42 (Figure 3b). Cloud amount was highly variable during the cooling period, with values oscillating daily between 0 and 8 (Figure 3c).

The saturation vapour pressure of thin snowpacks was relatively high at the beginning of the cooling period, when the temperatures were warmer (Figure 4a). Values were higher at the bottom of the snowpack, with a

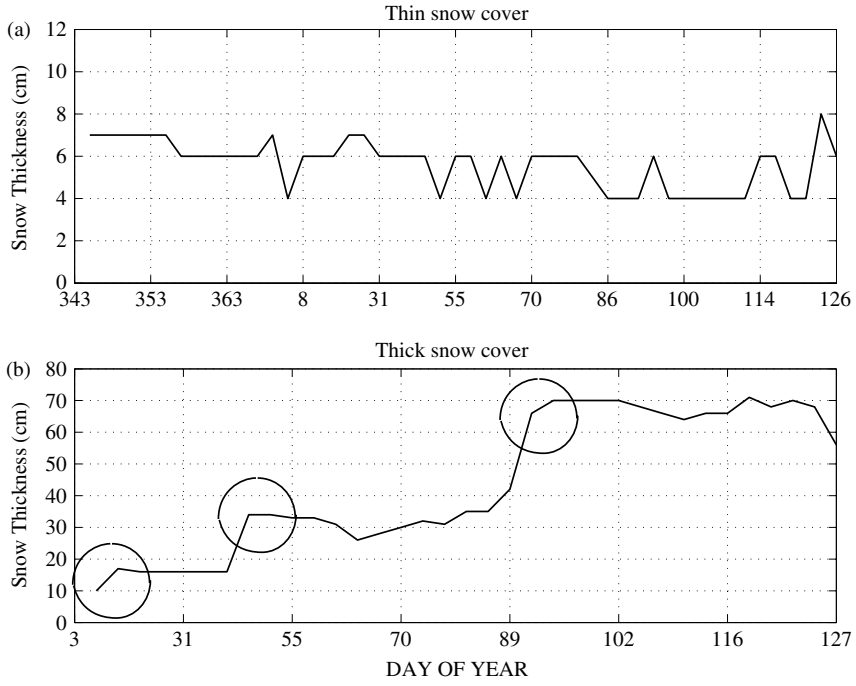

Figure 2. Snow thickness evolution for (a) thin and (b) thick snow covers

DOI: 10.1002/hyp

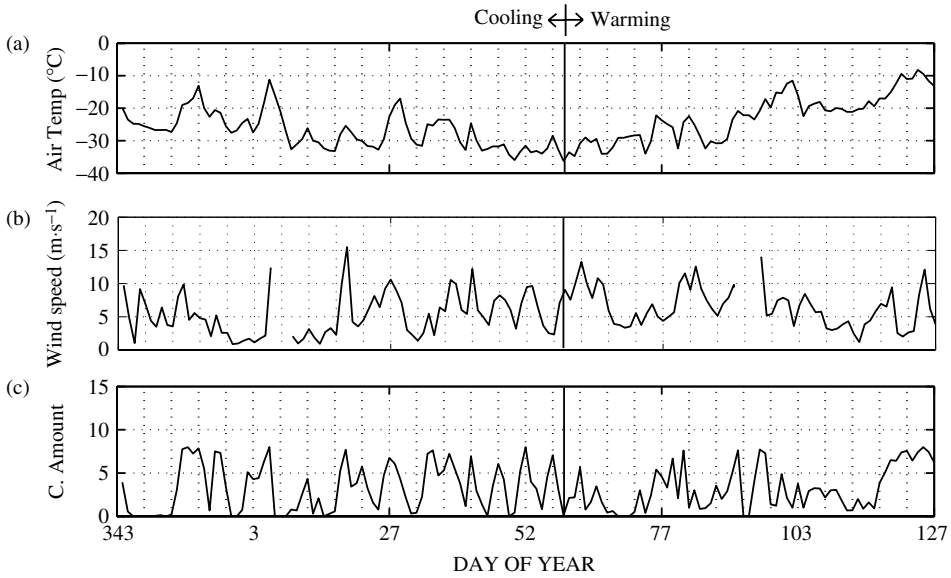

Figure 3. Daily averaged observation of (a) air temperature, (b) wind speed and (c) cloud amount

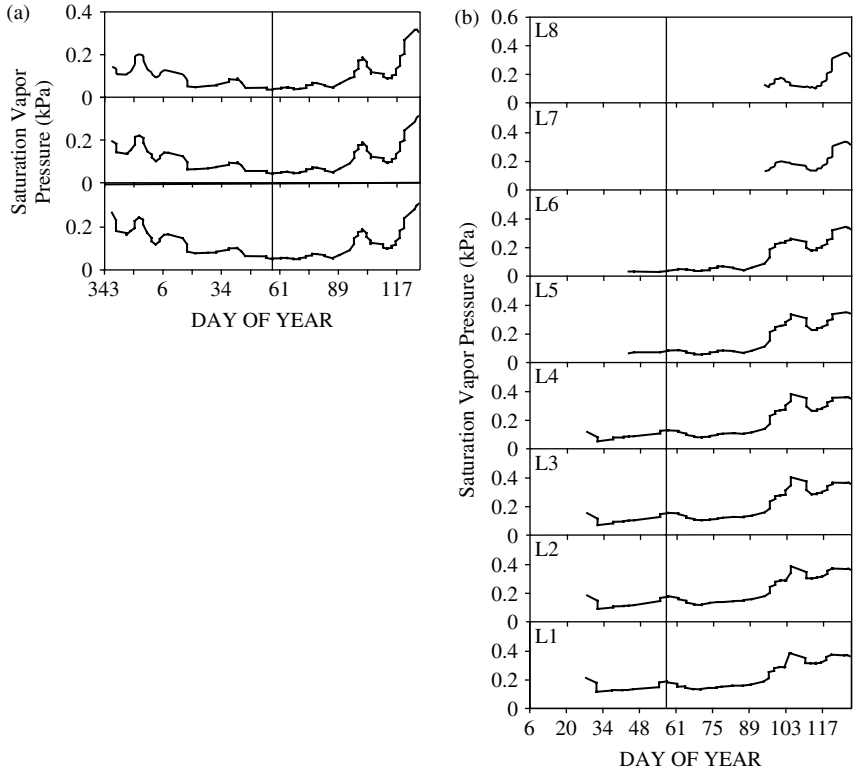

Figure 4. Evolution of the saturation vapour pressure e_{si} for (a) thin and (b) thick snow covers

maximum of 0·3 kPa. Two marked increases occurred, between days 350 and 360 and between days 5 and 10 (Figure 4a). Values varied between 0·150 kPa for L1 and 0·1 kPa for L2 to L4 (Figure 4b).

The daily averaged net radiation Q^* was highly variable during the cooling period, with values varying between 0 and -50 W m^{-2}; no significant trend was observed for this period (Figure 5a). Daily averaged downwelling (Figure 5b) and upwelling (Figure 5c) shortwave radiation measurements ($K\downarrow$ and $K\uparrow$) were very low during the cooling period. However, values increased throughout this period, with a maximum of 100 W m^{-2} on day 58. Downwelling longwave radiation (Figure 5d) measurements $L\downarrow$ were highly variable during the cooling period, reaching a minimum daily average of approximately 130 W m^{-2} on day 31. Upwelling longwave radiation $L\uparrow$ demonstrated less daily variation throughout this period, averaging approximately 200 W m^{-2} (Figure 5e).

Thin snow cover physical properties evolution. Snow grain size remained practically unchanged between days 348 and 34 (Figure 6a). A small decrease was noticed

DOI: 10.1002/hyp

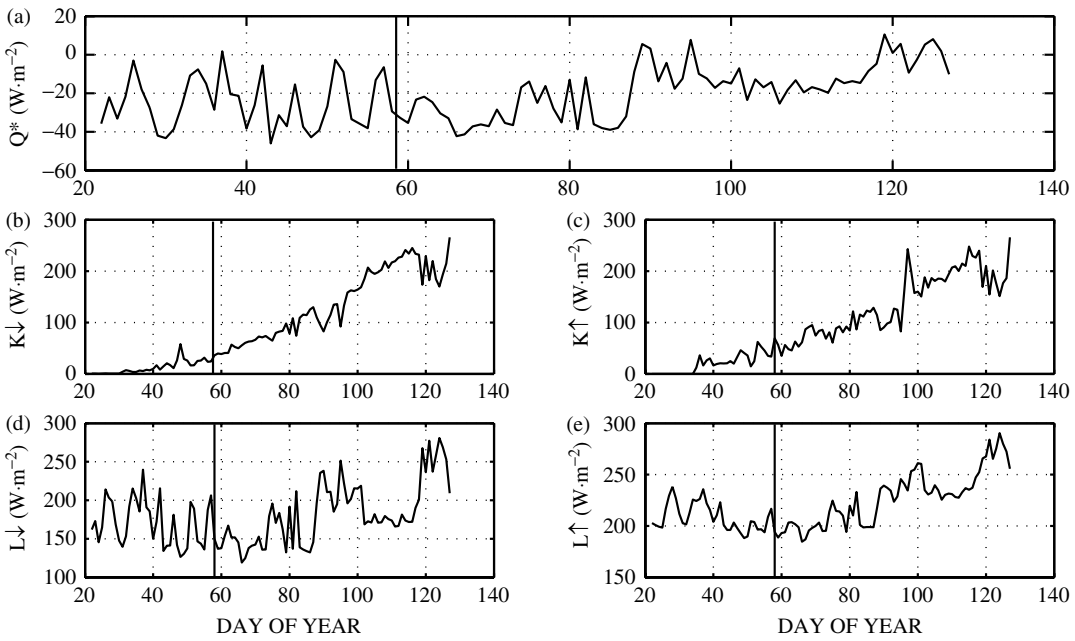

Figure 5. Daily averaged measured (a) net radiation, (b) downwelling longwave radiation, (c) upwelling longwave radiation, (d) downwelling shortwave radiation, and (e) upwelling shortwave radiation

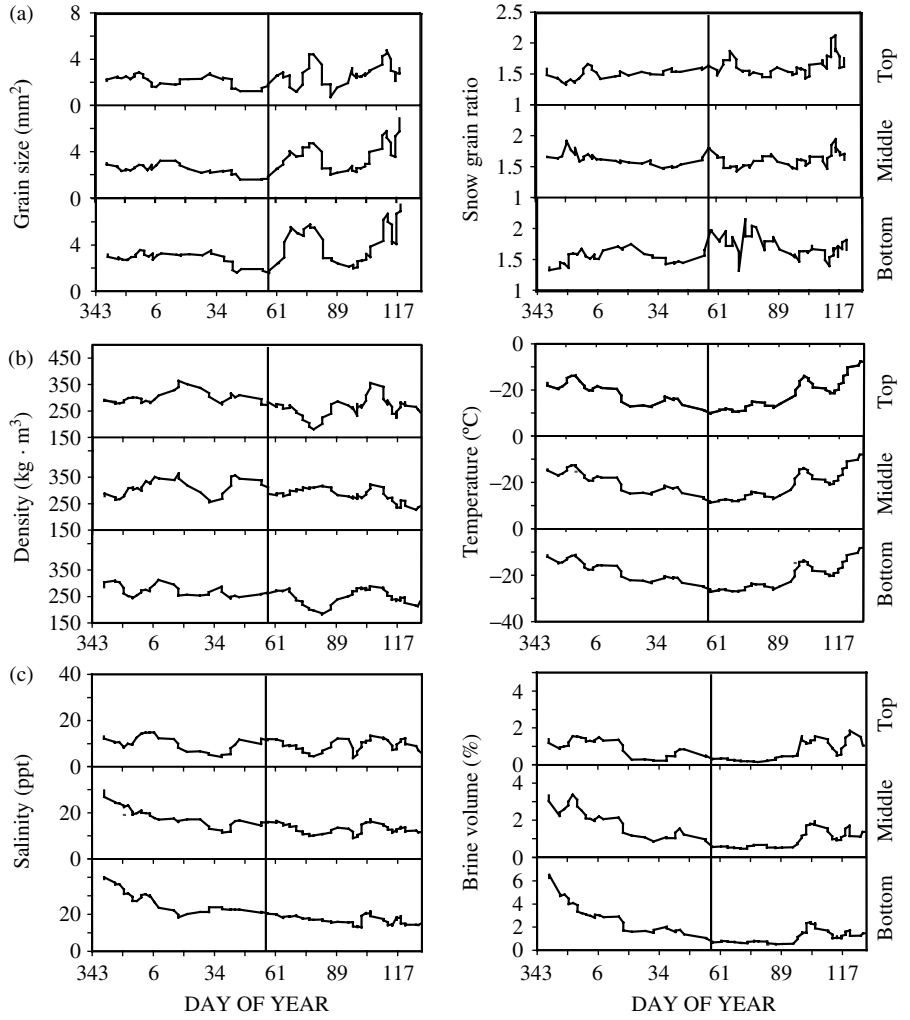

Figure 6. Evolution of thin snow cover: (a) grain size and ratio; (b) density and temperature; (c) salinity and brine volume

DOI: 10.1002/hyp

between days 34 and 59, where the size reached a minimum for the top, middle and bottom layers. Higher values were measured at the bottom layer, with grain size varying between 2 and 4 mm^2. Grain size in the middle and top layers varied between 1 and 2·5 mm^2. The snow grain ratio (major/minor axis ratio) did not change noticeably for the top layer (Figure 6a). Values in the bottom layer increased during the start of the cooling period, then levelled off following day 25. Grain shape in the middle layer was stable throughout the cooling period, whereas in the top layer the ratio tended to increase, although not significantly (Figure 6a).

Minimum $\delta T/\delta_L$ observations were coincident with warming temperature periods (i.e. days 357, 10 and 37) and low variation in saturation vapour pressure layer gradient $\delta e_{si}/\delta_L$ at the bottom snow–sea ice transition (Figure 7a and b). With small $\delta T/\delta_L$ and $\delta e_{si}/\delta_L$ at the bottom of the snowpack (i.e. low gradients), no vapour is expected to move upward, despite the presence of liquid water (Sturm and Benson, 1997) measured between days 34 and 48 (Figure 7c). Therefore, relatively stable grain size and low ratio (Figure 6a) values were observed during this cooling period.

Between days 348 and 15, the density increased for the top and middle layers, and then decreased until day 34 (minimum values for the cooling period in Figure 6b). Maximum temperatures were measured on day 357 at −10 °C, −10·1 °C and −9·2 °C for the top, middle and bottom layers respectively; minimum temperatures were recorded on day 59, with values of −30·2 °C, −28·6 °C and −26·1 °C respectively (Figure 6b).

Maximum density values at the top layer were reached on day 20, where winds were the strongest at 15 m s^{-1}. Wind breaks the snow crystals into rounded-shaped grains, creating high-density surface layers (Figure 3b). This mechanical process decreases the fraction of air in the layer, thus increasing the density, as observed in Figure 6b (e.g. Kotlyakov, 1961; Barber *et al*., 1995; Sturm *et al*., 2002; Mundy *et al*., 2005). The decrease in the top and middle layers between days 20 and 34 is associated with fresh falling snow (7·2 mm total precipitation) and low winds (average of 2·8 m s^{-1} between days 30 and 35). The increase between days 35 and 45 is also related to strong winds, which increased from an average of 2·8 m s^{-1} to 7·8 m s^{-1} between days 36 and 43.

A decrease in salinity was observed throughout the cooling period for the middle and bottom layers (Figure 6c). Minimum values were measured between days 31 and 37 for the middle layer and were observed between days 17 and 20 for the bottom layer. Brine volume (per cent) also decreased until day 59. However, brine volume reached a peak on around day 360 in the top and middle layers (Figure 6c).

Salinity decreased throughout the cooling period for all top, middle and bottom layers (Figure 6c). When sea ice forms, salts are rejected from the ice matrix towards both the atmosphere and ocean through the process of segregation (e.g. Weeks and Ackley, 1986; Eicken, 2003). Therefore, young snow covers over forming sea ice can have high salinity values that decrease afterwards with gravity drainage. Brine volume will respond proportionally as the cooling period evolves, further decreasing due to decreasing temperatures. However, for the top and middle layers we measured an increase in brine volume between days 348 and 15, which was coincident with warming temperatures (Figure 6b) over the same period, due to the sensitivity of brine to the colder temperatures of these upper layers (e.g. Frankenstein and Garner, 1967; Cox and Weeks, 1982).

Thick snow cover physical properties evolution. Snow grain size was unchanged for layers L1 to L4 for all of the cooling period (Figure 8). When layers L5 and L6 were deposited on day 42, the grain size remained stable in all layers until day 59, with average grain size values of 2 mm^2 for L1 and 0·5 mm^2 for L6. The snow grain ratio did not change during the cooling period for layers L1 to L4 (Figure 8).

We measured stable $\delta T/\delta_L$ at all layers throughout the vertical profile (Figure 9a). Furthermore, there was no substantial increase of $\delta e_{si}/\delta_L$, coincident with negligible wetness for L2 to L6 (Figure 9b). Therefore, liquid water

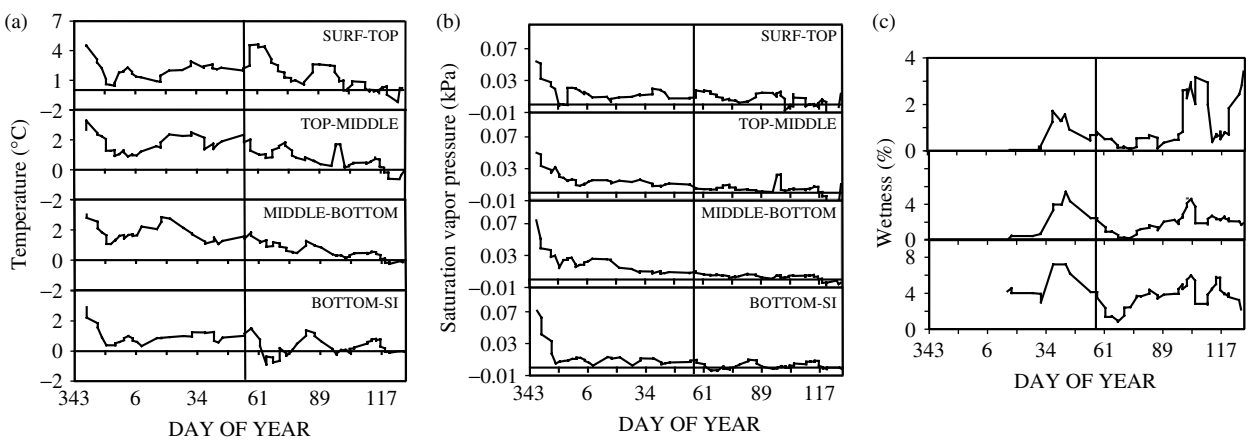

Figure 7. Evolution of thin snow cover: (a) temperature layer gradient; (b) saturation vapour pressure gradient; (c) wetness

DOI: 10.1002/hyp

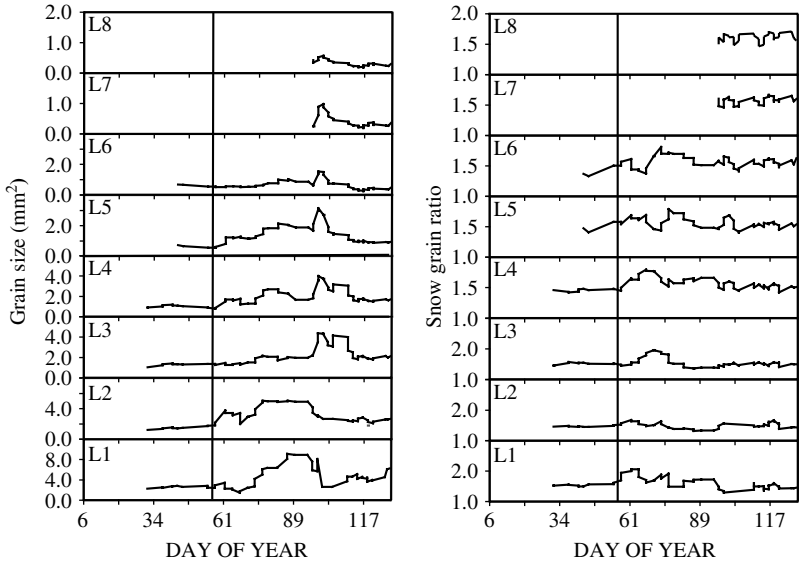

Figure 8. Evolution of thick snow cover grain size and ratio

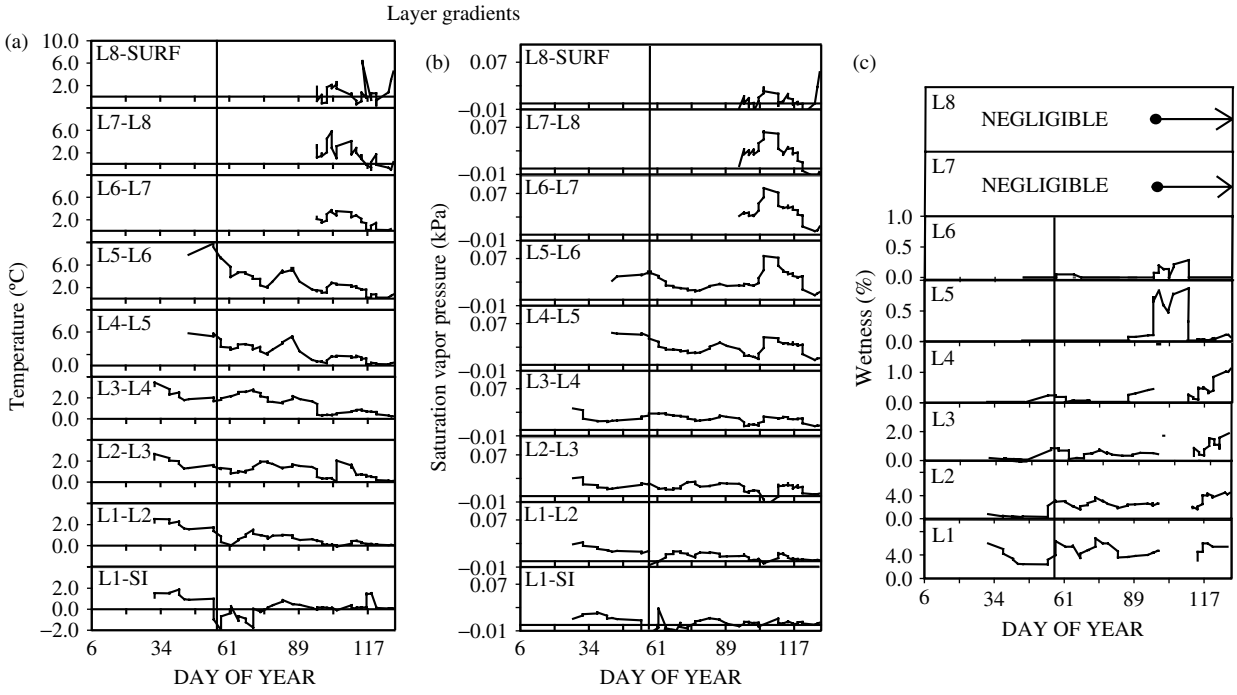

Figure 9. Evolution of thick snow cover: (a) temperature layer gradient; (b) saturation vapour pressure gradient; (c) wetness

was available in L1 (Figure 9c), but no temperature gradient was available to drag this moisture upward within the snowpack (i.e. no kinetic growth).

Snow density was unchanged for layers L1 to L4 during the cooling period (Figure 10). Values varied between 300 kg m^{-3}, 350 kg m^{-3} and 225 kg m^{-3} for L1, L4 and L6 respectively. The temperature remained stable throughout the vertical profile, with values varying between $-18\,^{\circ}C$ and $-25\,^{\circ}C$ for L1 and L6 respectively (Figure 10).

Salinity, on average, increased between days 42 and 59 for L1, L2 and L3 when L5 and L6 were deposited (Figure 11). Brine volume decreased for the first half of the cooling period at L1, with a minimum value approaching 1%. Values increased afterwards until day 59. Brine volume increased slightly at L2 and L3, but was relatively stable at L4 to L6, with values below 0·25% (Figure 11).

Warming period

Meteorological observations, layer gradients and energy fluxes. Throughout the warming period (between days 60 and 127), the averaged daily temperature increase was $+0{\cdot}35\,^{\circ}C$, with marked increases following days 88 and 101 (Figure 2a). Throughout the warming period, the averaged daily temperature increase was $+0{\cdot}35\,^{\circ}C$. Strong winds were recorded on days 62, 82, 84, 95 and 126, where recorded speeds were over 10 m s^{-1}. The last

DOI: 10.1002/hyp

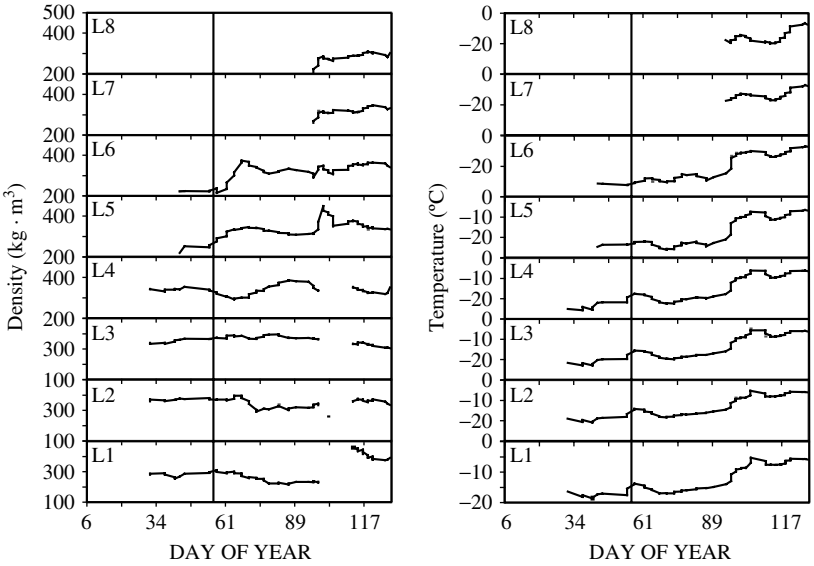

Figure 10. Evolution of thick snow cover density and temperature

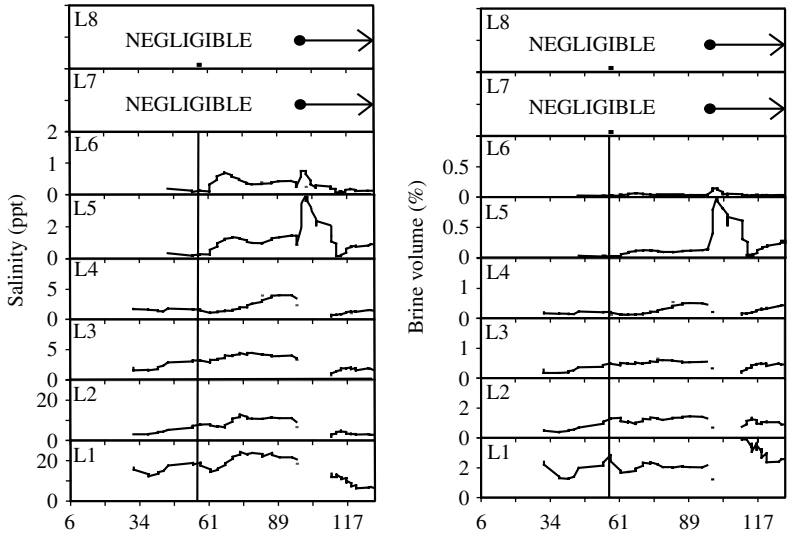

Figure 11. Evolution of thick snow cover salinity and grain size

snow redistribution event on day 91 (Figure 2b) was coincident with the strong winds measured between days 90 and 95 (Figure 3b). Low cloud amounts were observed at the beginning of the warming period. However, dense overcast periods were observed on days 76–81, 91, 95 and 118–127 (Figure 3c).

The saturation vapour pressure remained stable during the cooling period for thin snow until day 89, where a marked strong increase was observed (Figure 4a). This increase continued until day 103, where e_{si} values decreased until day 117 in all layers. Thick snow cover e_{si} values were also quite stable until day 95, where the increase occurred through to day 103 (Figure 4b).

The net radiation Q^* values at the beginning of the warming period were quite low, averaging $-32{\cdot}8$ W m^{-2} between days 59 and 72 (Figure 5a). A significant increase was measured between days 85 and 90, where values reached 0 W m^{-2}. The warming period was also characterized by a steady increase in shortwave radiation $K\downarrow$ and $K\uparrow$, with maximum values over 250 W m^{-2} on days 116 and 127 (Figure 5b and c). Both $L\downarrow$ and $L\uparrow$ increased during the warming period, where maximum values near 300 W m^{-2} were reached on day 124 (Figure 5d and e).

Thin snow cover physical properties evolution. Snow grain size was characterized by a marked increase at the beginning of the warming period in all three layers between days 59 and 91 (Figure 6a). The rate of growth for this period was steady and highest in the bottom layer. A growth rate of $0{\cdot}03$ mm·day^{-1} was measured in the top layer and $0{\cdot}25$ mm·day^{-1} for the bottom layer. Therefore, the bottom-layer snow grains grew about eight times faster than near the surface, where the temperature and wetness values were much lower. Inversely, the period between days 75 and 89 was marked by a significant decrease of $-0{\cdot}07$ mm day^{-1} for the

DOI: 10.1002/hyp

top layer and $-0{\cdot}24$ mm day^{-1} and the middle layer. Snow grain ratios were more variable during the warming period (Figure 6a). Values increased with increasing grain size between days 59 and 70 only for the top and middle layers, and then decreased to values around 1·5 until day 103. For the bottom layer, the increase was measured between days 59 and 75, where values jumped from 1·5 to 2·0 on average, coincidently with increasing grain size. This change was indicative of kinetic grain growth with highly faceted crystal formation (Colbeck, 1982).

The increase in grain size due to kinetic growth at the beginning of the warming period resulted from the increase in wetness and $\delta T/\delta_L$ between days 65 and 85 that initiated the vapour flow (Figure 7a and c). However, the decrease in grain size observed between days 89 and 103 was attributed to destructive metamorphism. Destructive metamorphism is the process in which the edge of a snow grain sublimates then recrystallizes towards the centre of the snow grain because the vapour pressure on a convex area is much higher than that in a concave area (Colbeck, 1997; Granberg, 1998). Such mass redistribution would decrease snow grain area, but not necessarily its volume.

Layers that are characterized with rounder shapes result from destructive metamorphism, resulting in reduced fractional air volume when the snowpack resettles. Thus, an increase in density would result, which was observed between days 82 and 111 in the top and bottom layers. Snow density was variable throughout the warming period (Figure 6b). For the top layer, a decrease was measured for the first part of the warming period, where values reached a minimum just over 150 kg m^{-3} around day 80. Density then increased between days 78 and 103, where maximum values were just over 350 kg m^{-3}. Volume temperatures increased significantly throughout the warming period, with a peak on day 103 for all three layers (Figure 6b). Maximum values were measured on day 125, where temperatures reached $-10\,^{\circ}$C and above in all layers.

The decrease in densities in the top and bottom layers between days 59 and 75 (Figure 6b) can be explained by either an increase in grain size, which can affect all layers, or new snow deposition, which affects the surface layers. The minimum in density occurred on day 76, as 0·7 mm of snowfall was recorded between days 59 and 76 affecting surface densities. However, the decrease in density in the bottom layer was attributed to the increase in grain size that increases the air volume fraction through the observed kinetic growth and associated vapour mass diffusion. The highest density values for all layers were observed just after day 103, which was associated with strong increases in temperature (Figure 3a) and wetness (Figure 7c).

Salinity was highly variable for the top layer, with fairly low values averaging 10 ppt (Figure 6c). Values decreased until day 75 for both the top and middle layers, but the bottom layers decreased until day 100. An increase in all layers was measured on day 103, where averaged maximum salinity values of 13 ppt, 17 ppt and 21 ppt were reached for the top, middle and bottom layers respectively. Brine volume was stable and low between days 59 and 95 (Figure 6c). An increase was measured for all three layers between days 95 and 103, where the maximum varied between 1·2% to just over 2%. This increase could have been due to an enhanced $\delta T/\delta_L$ (Figure 7c). The increase of salinity in these layers may have augmented the density and wetness increases, as brine-wetted snow has a depressed melting point (Granberg, 1998).

Thick snow cover physical properties evolution. There was a marked increase in grain size between days 59 and 85 from layers L1 to L6 (Figure 8). The snow grain growth rate for this period was larger in the bottom layer ($0{\cdot}48$ mm·day^{-1}) than the top layer ($0{\cdot}02$ mm·day^{-1}). Snow grains tended to decrease in size in L1 and L2 after day 85, reaching a minimum on day 103. Interestingly, grain size in L3–L6 increased after day 103. The snow grain ratio was variable in L1, but decreased towards day 127 (Figure 8). A slight increase was observed in L3 and L4 between days 59 and 70, but then values decreased until day 127 along with L5 and L6.

The increase in grain size was coincident with increasing values in water volume at L1 and L2 and coincidently with increasing $\delta T/\delta_L$ and $\delta e_{\mathrm{si}}/\delta_L$ from L4 to L6 (Figure 9a and b). However, a strong decrease started on day 97 at L1 and L2, which is the opposite to what occurred at L3 to L6, concurrent with the new snow deposition (L7 and L8). The decrease was due to seawater flooding of L1 and L2 that melted the snow grains. This situation occurred with the addition of L7 and L8, which increased the weight of the snowpack. This situation is not believed to be common in the Arctic, since the snow thickness is relatively thin in contrast to Antarctica, where thick snow covers are more common (e.g. Leppäranta and Hakala, 1992; Eicken, 2003). This type of flooding was also observed at other sampling areas east of the ship where snow fences intercepted snow covers over 70 cm. The flooding of layers L1 and L2 increased the brine volume (Figure 11), which moved upward in the snowpack due to an enhanced vapour flow. The saturation vapour pressure gradient increase was very strong between days 100 and 117 (Figure 9b), which coincided with the increase in salinity, brine and grain size. We would expect this increase to occur throughout the vertical profile, but the extraction of samples for density and salinity measurements was impossible due to the liquid consistency of the layers. However, it was possible to extract snow grains from the flooded surface.

Snow density from L1 to L3 was stable until day 97, where a marked increase occurred between days 97 and 111 coincidently with the deposition of layers L7 and L8 (Figure 10). Values increased from 275 kg m^{-3} to nearly 500 kg m^{-3}. The strong density increase in L6 at the beginning of the warming period (Figure 10) was due to strong winds that occurred between days 58 and 71 (Figure 3b). Wind densification and preferential

DOI: 10.1002/hyp

deposition on surface layers may have impacted layers below through compaction. The resultant density increase was observed at L4 between days 70 and 89. The same situation is observed at L5, where the increase in density between days 97 and 105 coincides with the deposition of L7 and L8. Snow temperature decreased between days 59 and 70 for L1 to L5, then increased until day 127, with a maximum value on day 103 for all layers (Figure 10).

The salinity in layers L1 to L4 increased between days 59 and 89 for L1 to L4, with values of 20 ppt and 5 ppt respectively (Figure 11). A peak in salinity at L5 and L6 coincided with the deposition of L7 and L8. The flooding of the basal layers increased the wetness and $\delta e_{\mathrm{si}}/\delta_L$ increased from L3–L5 to L8-surface transitions (Figure 9c), allowing migration of brine towards the top of the snowpack, as observed in Figure 11.

CONCLUSIONS

We characterized the fall to winter vertical profile evolution of thin and thick snowpack physical properties and associated meteorological forcing over land-fast first-year sea ice. From these data, we showed that snow physical and thermal properties evolve according to whether we categorize the system into 'cooling' or 'warming' periods. During the cooling period we observed only very small changes in the geophysical characteristics of the snowpack, except for salinity, which decreased throughout the cooling period. This snow desalination was stronger at the bottom of thin snowpacks, with a rate of $-0{\cdot}12$ ppt day^{-1} with an $R^2 = 0{\cdot}52$. We could not compare this rate with thick snow, as that sampling started later in the season. Net shortwave and longwave radiation did not appear to have a significant influence on either thin or thick snow covers, with high variability in $L\uparrow$ and $L\downarrow$ and low values for $K\uparrow$ and $K\downarrow$. The warming period initiated significant changes in the morphology of the snow grains for both thin and thick snowpacks (Figure 5, 'Meteorological observations, layer gradients and energy fluxes' section). The rate of growth was stronger for thick snowpacks ($0{\cdot}25$ mm day^{-1} and $0{\cdot}48$ mm day^{-1} for thin and thick snow respectively), where $\delta T/\delta_L$ and $\delta e_{\mathrm{si}}/\delta_L$ were larger (i.e. stronger vapour flow) and Q^* values near zero. The vapour pressure gradient is the main mechanism responsible for migration of brine upwards into the snowpack. Layers with brine volume are assumed to be saturated and, therefore, easily transferable to layers higher up with lower saturated pressure (i.e. lower temperature). Such mass movement had significant changes in snow grain morphology (Figures 6 and 7, 'Thin snow cover physical properties evolution' and 'Thick snow cover physical properties evolution' sections). These changes in grain shape impacted snow density and, therefore, the thermal properties. Hence, it is necessary to distinguish thin and thick snow when we want to assess their variability as winter progresses.

Flooding can occur with thick and heavy snowpacks, and its impact on the physical properties of the vertical profile is substantial. We showed that the input of seawater at the bottom of the snowpack increases the vertical saturation vapour pressure difference, initiating a strong vapour flow that increases the grain size towards the surface. Although this feature is not currently that common in the Arctic, it may be a scenario of increasing interest if ice thickness is reduced and snow thickness is increased in the future.

These results will assist in further development of snow geophysical and thermodynamic models for Arctic first-year sea-ice snow cover over the winter period. Work on developing empirical relationships between geophysical and electrical properties is being conducted in order to model these properties over the study period. As shown in this paper, the properties are linked together and the modelling will help us to understand better where (vertically) and when (temporally) these relationships are significant.

ACKNOWLEDGEMENTS

This work was financially supported by grants to DGB from the CASES NSERC Network, the Canada Foundation for Innovation (CFI) and the Polar Continental Shelf Project. We would like to thank the crew of the *CCGS Amundsen* for the essential logistical support throughout the study. We would like to thank Christina Blouw, Teresa Fisico, Owen Owens and John Iacozza from the University of Manitoba and Mark Christopher Fuller, Kris Konig and John Kudlak for tremendous assistance in the field sampling. Many thanks also to Tim Papakyriakou from the University of Manitoba and John Yackel from the University of Calgary for guidance and support throughout the experiment. Many thanks to Hardy Granberg from the University of Sherbrooke for providing comments that helped to improve this manuscript. Thanks also to the Centre for Earth Observation Science office staff for laboratory and logistical support.

REFERENCES

Arons EM, Colbeck SC. 1995. Geometry of heat and mass transfer in dry snow: a review of theory and experiment. *Reviews of Geophysics* **33**(4): 463–493.

Barber DG, Hanesiak JM. 2004. Meteorological forcing of sea ice concentrations in the southern Beaufort Sea over the period 1979 to 2000. *Journal of Geophysical Research* **109**: C06014.

Barber DG, Papakyriakou TN, LeDrew EF. 1994. On the relationship between energy fluxes, dielectric properties, and microwave scattering over snow covered first-year sea ice during the spring transition period. *Journal of Geophysical Research (Oceans)* **99**(C11): 22401–22411.

Barber DG, Reddan SP, LeDrew EF. 1995. Statistical characterization of the geophysical and electrical properties of snow on landfast first-year sea ice. *Journal of Geophysical Research* **100**(C2): 2673–2686.

Barber DG, Thomas A. 1998. The influence of cloud cover on the radiation budget, physical properties and microwave scattering coefficient of first-year and multi-year sea ice. *IEEE Transactions on Geoscience and Remote Sensing* **36**(1): 13.

Boer GJ, Flato G, Ramsden D. 2000. A transient climate change simulation with greenhouse gas and aerosol forcing: projected climate to the twenty-first century. *Climate Dynamics* **16**: 427–450.

Colbeck SC. 1982. An overview of seasonal snow metamorphism. *Reviews of Geophysics and Space Physics* **20**(1): 45–61.

Colbeck SC. 1993. The vapor diffusion coefficient for snow. *Water Resources Research* **29**(1): 109–115.

Colbeck SC. 1997. *A review of sintering in seasonal snow*. CRREL Report, 97-10; 1–11.

Comiso JC. 2002. A rapidly declining perennial sea ice cover in the Arctic. *Geophysical Research Letters* **29**: 17-1–17-4. DOI: 1029/2002GL015650.

Cox GFN, Weeks WF. 1982. *Equations for determining the gas and brine volume in sea ice samples*. CRREL Report, 1–20.

Curry JA, Rossow WB, Randall D, Schramm JL. 1996. Overview of Arctic cloud and radiation characteristics. *Journal of Climate*, **9**: 1731–1764, 1996.

Eicken H. 2003. From the microscopic, to the macroscopic, to the regional scale: growth, microstructure and properties of sea ice. In *Sea Ice: An Introduction to its Physics, Chemistry, Biology and Geology*, Thomas DN, Dieckmann GS (eds). Blackwell: Oxford, UK; 22–81.

Eicken H, Fischer H, Lemke P. 1995. Effects of the snow cover on Antarctic sea ice and potential modulation of its response to climate change. *Annals of Glaciology* **21**: 369–376.

Fisico T. 2005. Section 3·3. Meteorological observations. In *CASES 2003–2004 field summary*, Langlois A, Fisico T, Galley R, Barber DG (eds). CEOS-TEC-2004-09-01; 70–110.

Flato GM, Boer GJ. 2001. Warming asymmetry in climate change simulations. *Geophysical Research Letters* **28**: 195–198.

Frankenstein G, Garner R. 1967. Equations for determining the brine volume of sea ice from −0·5 to −22·9 degrees C. *Journal of Glaciology* **6**(48): 943–944.

Granberg H. 1998. Snow cover on sea ice. In *Physics of Ice-Covered Seas, vol. 2. Lecture Notes from a Summer School in Savonlinna*, Leppäranta M (ed.). University of Helsinki Press: 605–649.

Hanesiak J, Barber DG, Flato GM. 1999. Role of diurnal processes in the seasonal evolution of sea ice and its snow cover. *Journal of Geophysical Research* **104**(C6): 13593–13603.

Houghton JT, Ding Y, Griggs DJ, Noguer M, van der Linden PJ, Dai X, Maskell K, Johnson CA (eds). 2001. *Climate Change 2001: The Scientific Basis*. Cambridge University Press: New York.

Kotlyakov VM. 1961. *The Snow Cover of the Antarctic and its Role in the Present-Day Glaciation of the Continent*. Israel Program for Scientific Translation.

Leppäranta M, Hakala R. 1992. The structure and strength of first-year ice ridges in the Baltic Sea. *Cold Regions Science and Technology* **20**: 295–311.

Li W, Stamnes K, Chen B, Xiong X. 2001. Snow grain size retrieved from near-infrared radiances at multiple wavelengths. *Geophysical Research Letters* **28**(9): 1699–1702.

Massom R, Eicken H, Haas C, Jeffries MO, Drinkwater MR, Sturm M, Worby AP, Wu X, Lytle VI, Ushio S, Morris K, Reid PA, Warren SG. 2001. Snow on Antarctic sea ice. *Reviews of Geophysics* **39**(3): 413–445.

Maykut GA, Church PE. 1973. Radiation climate of Barrow, Alaska, 1962–66. *Journal of Applied Meteorology* **12**: 620–628.

Mellor M. 1977. Engineering properties of snow. *Journal of Glaciology* **19**: 15–66.

Moore DS, McCabe GP. 1993. *Introduction to the Practice of Statistics*, 2nd edition. Purdue University/W.H. Freeman.

Mundy CJ, Barber D, Michel C. 2005. Variability of snow and ice thermal, physical and optical properties pertinent to sea ice algae biomass during spring. *Journal of Marine Systems* **58**: 107–120.

Rogers RR, Yau MK. 1989. *A Short Course in Cloud Physics*, 3rd edition. Butterworth-Heinemann.

Serreze MC, Barry RG, Walsh JE. 1995a. Atmospheric water vapor characteristics at 70°N. *Journal of Climate* **8**: 719–731.

Stroeve JC, Serreze MC, Fettere F, Arbetter T, Meier W, Maslanik J, Knowles K. 2005. Tracking the Arctic's shrinking ice cover: another extreme minimum in 2004. *Geophysical Research Letters* **32**: L04501. DOI: 10.1029/2004GL021810.

Sturm M, Benson CS. 1997. Vapour transport, grain growth and depth-hoar development in the subarctic snow. *Journal of Glaciology* **43**(143): 42–59.

Sturm M, Holmgren J, König M, Morris K. 1997. The thermal conductivity of seasonal snow cover. *Journal of Glaciology* **43**(143): 26–41.

Sturm M, Holmgren J, Perovich DK. 2002. Winter snow cover on the sea ice of the Arctic Ocean at the Surface Heat Budget of the Arctic Ocean (SHEBA): temporal evolution and spatial variability. *Journal of Geophysical Research* **107**(C10): 23,1–23,16. DOI: 10.1029/2000JC000400.

Vowinkel E, Orvig S. 1970. The climates of the North Polar basin. In *Climates of the Polar Region*, Orvig S (ed.). Elsevier: 129–226.

Warren SG. 1982. Optical properties of snow. *Reviews of Geophysics and Space Physics* **20**: 67–89.

Warren SG, Rigor IG, Untersteiner N, Radionov VF, Bryazgin NN, Aleksandrov YI, Colony R. 1999. Snow depth on Arctic sea ice. *Journal of Climate* **12**: 1814–1829.

Weeks WF, Ackley SF. 1986. The growth, structure and properties of sea ice. In *The Geophysics of Sea Ice*, Untersteiner N (ed.). NATO ASI Series B: Physics vol. 146. Plenum: New York; 9–164.

Wu X, Budd WF, Lytle VI, Massom RA. 1999. The effect of snow on Antarctic sea ice simulations in a coupled atmosphere–sea ice model. *Climate Dynamics* **15**: 127–143.

Xin J, Barber DG. 2006. An assessment of the sensitivity of cloud radiative forcing on the initiation and rate of melt over snow covered landfast first year sea ice with Terra/MODIS data. *Hydrological Processes* in press.

Yang Z-L, Dickinson RE, Hahmann AN, Niu G-Y, Shaikh M, Gao X, Bales RC, Sorooshian S, Jin JM. 1999. Simulation of snow mass and extent in global climate models. *Hydrological Processes* **13**: 2097–2113.

Zhou X, Li S. 2002. Phase functions of large snow melt clusters calculated using the geometrical optics method. In *Proceedings IEEE 2002 International Geoscience and Remote Sensing Symposium (IGARSS'02)*, Vol. I, 3576–3578.